2D Patterned Ion-Exhange Membranes Induce Electroconvection

Florian Roghmans[1], Elizaveta Evdochenko[1], Felix Stockmeier[1,2], Sven Schneider[1], Amel Smailji[1], Rahul Tiwari[2], Annabel Mikosch[2], Alexander Kühne[2], Andreas Walther[3], Ali Mani[4], and Matthias Wessling*[1,2]

[1]RWTH Aachen University, Chemical Process Engineering, Forckenbeckstraße 51, 52074 Aachen, Germany

[2]DWI - Leibniz Institute for Interactive Materials, Forckenbeckstraße 50, 52074 Aachen, Germany

[3]University of Freiburg, Institute for Macromolecular Chemistry, Stefan Meier Straße 31, 79104 Freiburg, Germany

[4]Stanford University,Department of Mechanical Engineering, Stanford, California 94305, USA

Keywords

Electrodialysis, Electroconvection, surface modification, microgels, inkjet printing

*corresponding author
manuscripts.cvt@avt.rwth-aachen.de

Abstract

Concentration polarization is a diffusion-limited phenomenon for ion transport in electrodialysis based desalination processes. Once a so-called limiting current is reached, the resistance of the system rises notably manifested as a plateau region in the current-voltage curves. For long it is hypothesized that altering the surface properties of the membrane can overcome the diffusional transport limitation by the induction of electroconvective vortices mixing up the laminar boundary layer. To systematically investigate the influence of geometrical and chemical membrane surface topology on the evolution of electroconvection, circular patterns of polystyrene, poly(2-vinylpyridine) and P2VP-microgels were inkjet printed on cation-exchange membranes. All types of patterns cause an insignificant increase in membrane resistance but they reduce the plateau lengths indicating the desired accelerated onset of electroconvection. In case of PS patterns, the drop in plateau length results in a small reduction in transport resistance for overlimiting currents. However, membranes modified with linear P2VP and P2VP microgel patterns do exhibit a significantly decreased resistance in this region at a simultaneous increase of the limiting current density. Direct numerical simulations support our interpretation that the surface charge of the printed patterns influences the direction of the vortices being advantageous during ion transport towards the membrane.

1 Introduction

Biological as well as synthetic membrane processes are limited by diffusional resistances at the membrane fluid interface resulting in polarized concentration profiles. In the field of synthetic membranes for technical applications such as desalination

and bioprocessing, the phenomenon of concentration polarization frequently hampers development and implementation. In pressure-driven membrane processes, such as reverse osmosis, nanofiltration and ultrafiltration, the convective flux towards the membrane at the feed side is higher than the diffusive back transport of rejected species. The flux through the membrane stagnates at the so-called critical flux even if the transmembrane pressure is increased. Concentration polarization also severely affects ion transport through ion-exchange membranes in electrodialysis systems. Here, an electrical potential applied over the membranes acts as the driving force. At low applied potentials, the resulting current scales linearly with the potential as seen in Figure 1 (a). When the potential is further increased, the diffusion boundary layer gets depleted due to higher transport numbers of counter ions in the ion exchange membrane as compared to the ones in the solution. This leads to a plateau region analogous to that appearing in pressure driven processes, where the current (the flux of ions) through the membrane cannot be increased.

As opposed to pressure-driven processes, in electrodialysis the current density suddenly increases once a threshold voltage is surpassed. Different phenomena are responsible for this so-called overlimiting current transfer [1, 2]. In most cases the evolution of electroconvection is the governing mechanism [1]. Here, hydrodynamical instabilities induce vortices at the membrane surface which mix the diffusion boundary layer. Therefore, new ions are transported to the membrane and higher ionic fluxes can be sustained. Many theoretical works have been conducted to understand the origin of the electroconvective fluxes and their influence on overlimiting mass transfer [3, 4, 5]. For the first time, the existence of these vortices was experimentally proven by Rubinstein et al. [6] and also visualized in an electrodialysis flow channel by Kwak et al.[7].

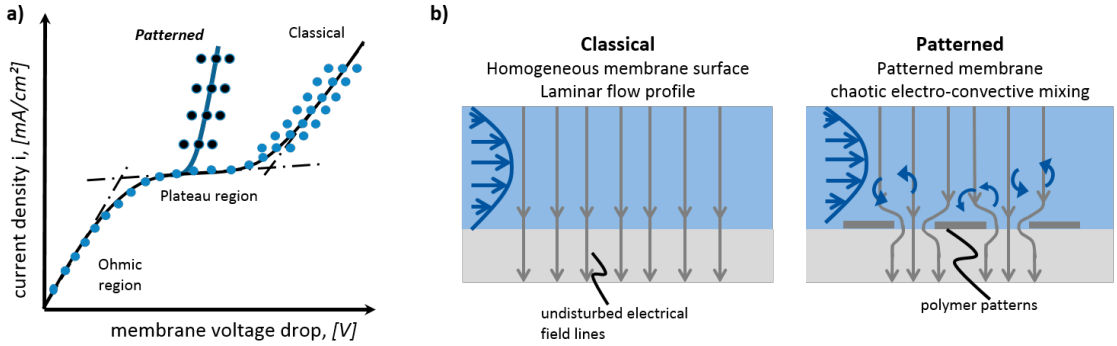

Figure 1: Scheme of a) a typical i-v curve and b) the electric field line distribution of patterned and unpatterned membranes.

De Valença et al. [8] further investigated the speed of vortices evolving at different stages of the ion depletion process. Druzgalski et al. [9] quantified the correlations between current density in the membrane and the normal velocity in the adjacent bulk fluid by examining 3D direct numerical simulation data. Their analysis also revealed that the enhancement in ion transport is dominantly contributed by large vortices with sizes in the order of the thickness of the boundary layer.

Electrical and geometrical inhomogeneities of the membrane surface were mathematically predicted to lead to an intensified onset of electroconvection and therewith a shortened plateau length [4, 10]. Figure 1 b) visualizes the reasoning behind the earlier onset of electroconvection: the deflection of the electrical field lines due to a heterogeneous membrane surface causes a tangential component which, in turn, induces an electrolyte slip, initiating and maintainig electroconvective vortices. Balster et al. [2] experimentally proved that chemical heterogeneity as well as micrometer-sized geometrical embossed undulations, indeed, may impact on the evolution of electroconvection resulting in a decreased plateau length. Nanometer-thick micrometer-sized polyelectrolyte patterns transferred through micro-contact printing on top of a membrane have the same effect on the emergence of electro-osmotic induced fluid instabilities [11]. Other works have shown that also hydropho-

bic surfaces lead to an intensified evolution of electro-convective vortices mixing the diffusion boundary layer[12, 13, 14]. Through direct numerical simulations, we have recently discovered a complex chaotic mixing behavior induced by impermeable patches [15]. Yet, little is known whether and how the surface charge and the structure of the patterns influence the onset of electro-convection.

Here, we report a new fabrication process for patterned ion exchange membranes based on ink-jet printing. Ink-jet printing is a versatile method achieving an accurate deposition of polymers, particles or cells [16, 17, 18, 19]. Through the choice of the nature of the ink, very different surface functionalities can be applied. In membrane science, ink-jet printing has recently been used to modify composite membranes for desalination and water treatment [20]. Yet, the challenge in using ink-jet printing lies in finding appropriate properties of the ink to reproducibly print the structures. For instance, the use of a mixture of solvents tailors their evaporation rate to produce the desired structures [17, 21]. Another parameter influencing the printed structures is the hydrophobicity of the substrate[22]. For instance, printing of hydrophobic patches on hydrophilic polymer films that swell in a solvent is an experimental challenge, addressed below.

With respect to printed patterns on electrodialysis membranes, we investigate three very different materials: dots printed from (a) hydrophobic linear polystyrene (PS) bearing a negative zeta potential (b) linear poly(2-vinylpyridine) (P2VP) polymers having a positive zeta potential and (c) colloidal P2VP microgels. Polystyrene and P2VP are relevant as they represent the situation in which the influence of the surface charge is depicted. Colloidal microgels are relevant as they can form colloidally assembled microstructures. They are crosslinked, water-swollen polymer entities that swell or deswell due to different stimuli such as changes in pH, temper-

ature or ionic strength [23, 24, 25, 26]. A recently reported application in the field of membrane science is the generation of thermoresponsive hollow fiber filtration membranes by coating them with microgels [27, 28]. The potential of microgels to influence ion transport in electrochemical deionization processes is relevant as well. Their effect on monovalent ion selectivity was investigated in our recent paper [29]. Moreover, their ability to exhibit distinct properties under the effect of external stimuli opens a variety of possibilities to reversibly tune ion transport according to the needs of a specific electro-membrane process. One possibility to tailor the ion transport in these processes by means of microgels is shown below. In this paper, we functionalize the surface of Nafion 117 cation exchange membranes with ink-jet printed dotted PS and P2VP patterns as well as colloidal P2VP microgels patterns. This represents the first systematic experimental and simulation study investigating the influence of dot nature and surface charge, dot spacing and dot density on the accelerated onset of electroconvection.

2 Experimental details

2.1 Materials

The membranes used in the experiments are commercially available Nafion 117 cation-exchange membranes (DuPont, USA) either as received or modified with ink-jet printed patterns of linear polystyrene (PS), linear poly(2-vinylpyridine) (P2VP) polymers or crosslinked P2VP microgels. For the printing procedure, 1 wt% of either linear PS (average molecular weight 280 kDa) or linear P2VP polymers (average molecular weight: 37.5 kDa) were dissolved in a mixture of (60/40) wt% ethyl acetate and acetophenone. All chemicals were purchased from Sigma-Aldrich. P2VP

microgels were synthesized via surfactant free emulsion polymerization [29] with a crosslinking degree of 1:100. Absorbed on a surface, the microgels have a thickness of 300 nm in swollen state. For the patterning, the microgels were diluted to 0.05 wt% in ultra pure water. The differently modified membranes were characterized and compared with pristine membranes of the same batch.The ink-jet printing was performed with an Autodrop Compact 2.21 ink-jet printer with a MD-K-140 print head (microdrop Technologies, Germany).

2.2 Electrochemical Characterization of the Membranes

2.2.1 Current voltage measurements

The influence of different polymer patterns on the onset and intensity of electroconvection was characterized by current-voltage polarization curves and chronopotentiometric measurements. The experiments were done in a six compartment electrodialysis cell [30]. The compartments surrounding the investigated membranes were filled with 0.1 M NaCl solution. Prior to the experiments, the membranes were equilibrated in this solution for at least 12 hours. All measurements were executed using the four-electrode method. Two working electrodes were used to apply the voltage inducing electric current, whereas the voltage drop over the Nafion reference or ink-jet printed membranes was obtained by two calomel reference electrodes (ProSense B.V., QM712X). To bring the reference electrodes as close as possible to the membrane surface, the electrodes were extended using Haber-Luggin capillaries. The electrolyte flow rate was kept constant at 0.5 L/min. During all experiments the temperature was maintained at 25 °C.

In the current-voltage measurements, the voltage at the working electrodes was increased stepwise with an Agilent 6634B power supply, every 30 s in the underlimiting

regime and every 60 s in the plateau and overlimiting regime. Conductivity and pH values were recorded in every compartment. These parameters as well as the current and voltage values were logged every second. No significant water splitting was registered throughout all experiments.

2.2.2 Data analysis of current voltage measurements

The resistance of the membrane/solution system in the ohmic regime was determined as the reciprocal of the slope of the current-voltage (i-V) curve in this regime. Here, the limiting current density (i_{lim}) was calculated by subtracting the ohmic part from the i-V curve. As a result of the subtraction, the ohmic part of the curve lies on the y-axis. With the beginning of the plateau regime, the reduced voltage drop starts to deviate from zero. Thus, this point is referred to as i_{lim}. To obtain the plateau length, a sigmoidal function was fitted to the reduced current-voltage curve to find its inflection point [31]. Knowing the membrane voltage drop at which the limiting and the overlimiting current densities are located, the plateau length is easily calculated by the difference between both values.

2.2.3 Chronopotentiometric measurements

Chronopotentiometric measurements enable the characterization of the time-evolution of the concentration polarization at the membrane surface. For this purpose a constant current is applied to the system and the voltage response is tracked [32, 33]. These measurements were executed with an IviumStat XR potentiostat (Ivium Technologies, the Netherlands). The current and voltage values were logged every 0.1 seconds. Chronopotentiometric curves can be divided into four parts [32]. First, after setting the current, the voltage rises instantaneously, reaching a value which reflects the ohmic membrane and solution resistance. In the second part, the voltage

increases only slightly with time. After a certain time, the voltage rises steeply as the polarization at the membrane surface intensifies. The time, corresponding to the inflection point during the steep voltage increase, is known as the transition time and it represents the time at which the salt concentration at the membrane surface approaches zero. From this point on, the ion flux is maintained by electroconvective fluxes in case electroconvection is the governing mass transfer mechanism of the overlimiting mass transfer. Finally, the response stabilizes to an average value with fluctuations representing the electro-convective mixing of the boundary layer. The transition time can be correlated to the current by means of the Sand equation[32]:

$$\tau = \frac{\pi D}{4}\left(\frac{c_b z F}{t^m - t^s}\right)^2 \frac{1}{i^2} \tag{1}$$

Where D is the Diffusion coefficient of the permeating ion, c_b is the bulk concentration, z the valency and F the Faraday constant. t^m and t^s stand for the ion transport numbers in the membrane and in the solution respectively.

When inhomogenoeus membranes are investigated, the current density has to be corrected by the fraction of conducting regions ϵ resulting in an increased current density in the conductive areas of the membrane[34]:

$$i_{local} = \frac{i}{\epsilon} \tag{2}$$

With this the Sand equation for inhomogeneous membranes can be written as:

$$\tau = \frac{\pi D}{4}\left(\frac{c_b z F}{t^m - t^s}\right)^2 \frac{1}{i_{local}^2} \tag{3}$$

A drawback of the Sand equation is that it only takes the diffusive ion transport into account. It was already mathematically and experimentally shown that experimentally determined transition times are always larger than the ones obtained by

the Sand equation [13, 14, 35]. Thus, electroconvective flows may already promote the ion transfer even before the membrane surface is fully depleted. In simulations of electroconvection at wavily structured membranes, Pham et al. [36] found that first vortices even occur in the underlimiting regime. Rubinstein et al. [37] showed that also any instability in the EDL leads to an onset of electroconvection already in the underlimiting region. Since the transition time is proportional to the inverse square of the current density, the product of the other parameters in the Sand equation can be seen as a constant which is proportional to the mass transfer coefficient describing the electro-diffusive as well as the convective contributions to ion transport. Merging these parameters into a single one leads to

$$\tau = K\frac{1}{i^2} \tag{4}$$

and

$$\tau = K_{local}\frac{1}{i_{local}^2} \tag{5}$$

respectively. Further, a mass transfer enhancement factor P can be defined as

$$P = \frac{K_{pat}}{K_{ref}} \tag{6}$$

where K_{pat} and K_{ref} represent the mass transfer constants at the patterned and the reference membranes respectively.

To determine the transition time of chronopotentiometric measurements, the inflection point of voltage response over time, the maximum of the first derivative, has to be found. Therefore, the derivative is approximated by forward differential quotients:

$$\frac{\partial U_m}{\partial t} \approx \frac{U_m(t+\Delta t) - U_m(t)}{\Delta t} \tag{7}$$

Δt, here 0.1 s, represents the time between two measuring points.

2.3 Simulations

To investigate the impact of patterned ion exchange membrane surfaces on the ion transport, two different 2D simulations of the membrane/solution system were performed in a finite element based commercial multiphysics package, COMSOL Multiphysics 5.3. Further details and schematic representations of the investigated domains of the two modells can be found in the supporting information of this paper.

2.3.1 Steady-State Modelling

The steady-state model investigates the influence of patterns on the ohmic behaviour and the limiting current. It neglects the influence of induced flow and the physics describing the onset of electroconvection. The system modelled consists of a membrane and two diffusion boundary layers. Both sides of the membrane is adjacent to NaCl solutions which are assumed to have uniform concentration of the bulk soltuion as an initial conditions.

The area covered by impermeable and uncharged patches was altered to mimic the experimental conditions. The set of equations to describe transport of N species through the diffusion boundary layers and the membrane is the following [38, 39]. For a better comparison with the experiments, all the equations are considered in the dimensional form.

$$0 = -\nabla j_i, \qquad \forall i = 1...N \tag{8}$$

Equation 8 is the conservation of ionic species, where j_i is the flux of species i described by the Nernst-Planck equation:

$$j_i = -D_i(\nabla c_i + z_i c_i \frac{F}{RT}\nabla\varphi), \tag{9}$$

where c_i and z_i are the concentration and valence of species i respectively, D_i is the diffusion coefficient, F is the Faraday constant, R is the ideal gas constant, T is the absolute temperature and φ is the electric potential.

$$\nabla^2\varphi = -\frac{F}{\varepsilon\varepsilon_0}\rho_e. \tag{10}$$

Equation 10 is Poisson's equation, where ε is the solution relative permittivity, ε_0 is the vacuum permittivity and ρ_e is the free electric charge density [38, 39]:

$$\rho_e = \sum_{i=1}^{N} z_i c_i. \tag{11}$$

To model the membrane domain, the diffusion coefficient D_i is altered by a coefficient α ($\alpha = 0.1$) to account for the membrane porosity and tortuosity of the diffusion path. In the Poisson equation, a term σ is added to the free electric charge density representing the membrane fixed charge groups [38, 39]. Hence, for the membrane domain, equations 9 and 10 have the form:

$$j_i = -\alpha D_i(\nabla c_i + z_i c_i \frac{F}{RT}\nabla\varphi), \tag{12}$$

$$\nabla^2\varphi = -\frac{F}{\varepsilon\varepsilon_0}(\rho_e + \sigma). \tag{13}$$

To obtain current-voltage curves, the electrical potential was step wise increased over the three domains until the limiting current density was approached. The total current density was calculated after each step. Then, the distribution of the counter-ions over the membrane thickness and in the diffusion boundary layers was analyzed in order to better understand the influence of the membrane coverage on

the resistance of the system.

2.3.2 Dynamic Modelling

For the description of electrokinetic flow at zero Reynolds number, a dynamic model was implemented in COMSOL, as described by Karatay et al.[40]. Here, the 2D computational domain consists of an electrolyte above a cation exchange membrane surface. The membrane is not included in the model. However, the boundary conditions are set to describe the behavior of the electrolyte right at the membrane surface.

The above mentioned equations 8, 9 and 10 are scaled in dimensionless form and were modified to depict the time dependency and convection[41]. The set of equations, outlined above, is extended by the Navier-Stokes-equation and the continuity equation for the electrolyte phases.

The modified Nernst-Planck and conservation equation result in:

$$\frac{\delta c_i}{\delta t} = -\nabla \cdot (c_i \mathbf{u} - D_i \nabla c_i - D_i z_i c_i V_T^{-1} \nabla \phi) \tag{14}$$

Here, $\mathbf{u}$ is the velocity vector in x and y direction and V_T is the thermal voltage ($V_T \approx 0.025\ V$) and ϕ the dimensionless representation of the applied voltage.

Poisson's equation is in nondimensional form:

$$-\nabla^2 \phi = \frac{c_c - c_a + sig}{2\epsilon^2} \tag{15}$$

Here, c_c and c_a refer to the cation and anion concentration, respectively. Sig is the concentration of fixed charge in the patches. It is set to 0 for all regions outside the patches. Furthermore, $\epsilon = \frac{\lambda_D}{L}$ is the dimensionless form of the Debye length λ_D

divided by the height of the domain L.

Druzgalski et al.[41] showed that the inertial term of the Navier-Stokes-equation can be neglected in this formulation. An incompressible fluid is described by:

$$0 = -\nabla p + \mu \nabla^2 \mathbf{u} - \rho_e \nabla \phi \tag{16}$$

and

$$\nabla \mathbf{u} = 0 \tag{17}$$

where p and μ are the pressure and the viscosity.

Four patches are spread equidistantly above the membrane surface bearing a static positive or negative charge. To mimic the different surface charge of the polymers used in the experiments, sig was set to be 0.01 c_{bulk} within the patches.

The applied potential was set to $\phi = 30V_T$ as a suitable high potential for the formation of vortices. The remaining variables are selected as suggested by Karatay et al.[40].

3 Results and discussion

3.1 Ink-jet printed patterns

The ink-jet printing of the dissolved linear PS and linear P2VP lead to homogenous polymer patterns after evaporation of the solvents. Figure 2 b) shows a membrane patterned with PS arrays with a coverage of 50%. The printing of the colloidal P2VP microgels results in dots with a non-confluent P2VP microgel monolayer showing a non-homogeneous distribution with a denser monolayer packing on the outer ring and lower packing in the center of the drop Figure 2 c). To be able to investigate the

influence of the membrane coverage on the onset of electroconvection, the distance between the polymer dots, was varied to obtain coverages within 25% and 50% (Figure 2 a). The diameter of the arrays was kept constant at 400 μm throughout all experiments. For the microgel patterns, it was not possible to coat the surface with more than 31% because of a significant swelling of the Nafion membranes when coming in contact with water.

For a better comparison of the colloidal P2VP microgels and the linear P2VP polymer in the further investigations, membranes were also printed with 25% and 31% of linear P2VP. The dots of the PS and P2VP had a thickness of about 2 microns. The dots of the microgels had a typical morphology shown in (Figure 2 c) with a monolayer having less lateral microgel density in the center and a ring of higher density on the outside.

3.2 Polystyrene polymer patterns on Nafion

Current-voltage (i-V) curves of the patterned membranes were measured to characterize their performance over a wide range of currents. Figure 3 a displays the i-V curves of the PS-patterned Nafion membranes in comparison to an uncoated reference. The membrane resistances in the ohmic region and the limiting current density vary only slightly, although the coverages are altered by up to 50 % (Table 1). This behavior was confirmed by stationary COMSOL simulations which serve to explain the experimental data (Figure 4). Since the electric field lines deflect in the solution from the impermeable patch towards the membrane, they also deflect inside the membrane, spreading into the region right behind the patterns (Figure 4 b). Thus, the ions also diffuse into the region behind the patterns, so that the actual unused membrane volume is much lower than the area covered by the non-conductive pat-

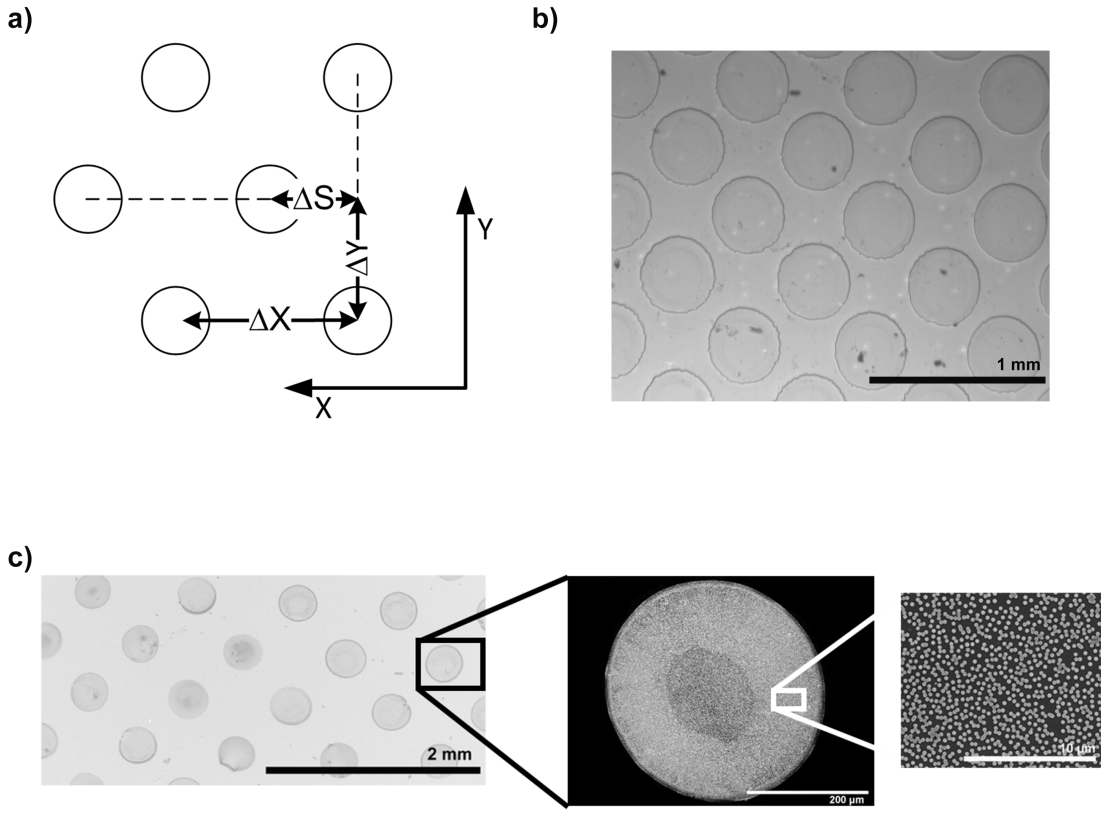

Figure 2: a) Scheme of the printed arrays. Printed patterns of b) polystyrene (PS) and c) of P2VP microgels of 400 μm diameter on a Nafion ion-exchange membrane.

terns implies.

Both the experiments and the simulations show the evolution of the plateau region of modified membranes already at lower current densities. In case of the patterned membranes, the earlier onset is caused by higher local current densities in the uncovered regions, which leads to an earlier depletion of the boundary layer.

All investigated PS coatings improve the mixing of the boundary layer, as indicated by decending plateau lengths in Figure 3 b. The degree of coverage or, more precisely, the distance between the patterns has a decisive impact on the evolution and efficiency of the electroconvective vortices. Davidson et al.[15] showed by 2D simulations, which investigated the evolution of electroconvection at patterned membranes, that the threshold potential for the onset of stable vortices is lower. These vortices arise in counter-rotating pairs of the same period as the pattern itself, thereby changing in size and efficiency of mixing the boundary layer. Thus, in this experimental case the inter-pattern distance at 35 % coverage leads to the most efficient mixing reflected in the minimum plateau length and the biggest reduction of the overall resistance in the overlimiting region. However, this resistance was only slightly decreased by 5 %. The above mentioned 2D simulations revealed an optimum in overlimiting mass transfer at 60 % coverage. The difference between the experiments and the simulations might be caused by the different ratios of pattern sizes to flow channel height in each system. Another essential difference is the neglected third dimension in the simulations. In a more recent paper Duzgalski et al.[9] did a comparison of 2D and 3D simulations. 2D simulations underpredict the charge density in the mixed zone and the net current through the system.

Chronopotentiometric measurements depict the dynamics of ion depletion and

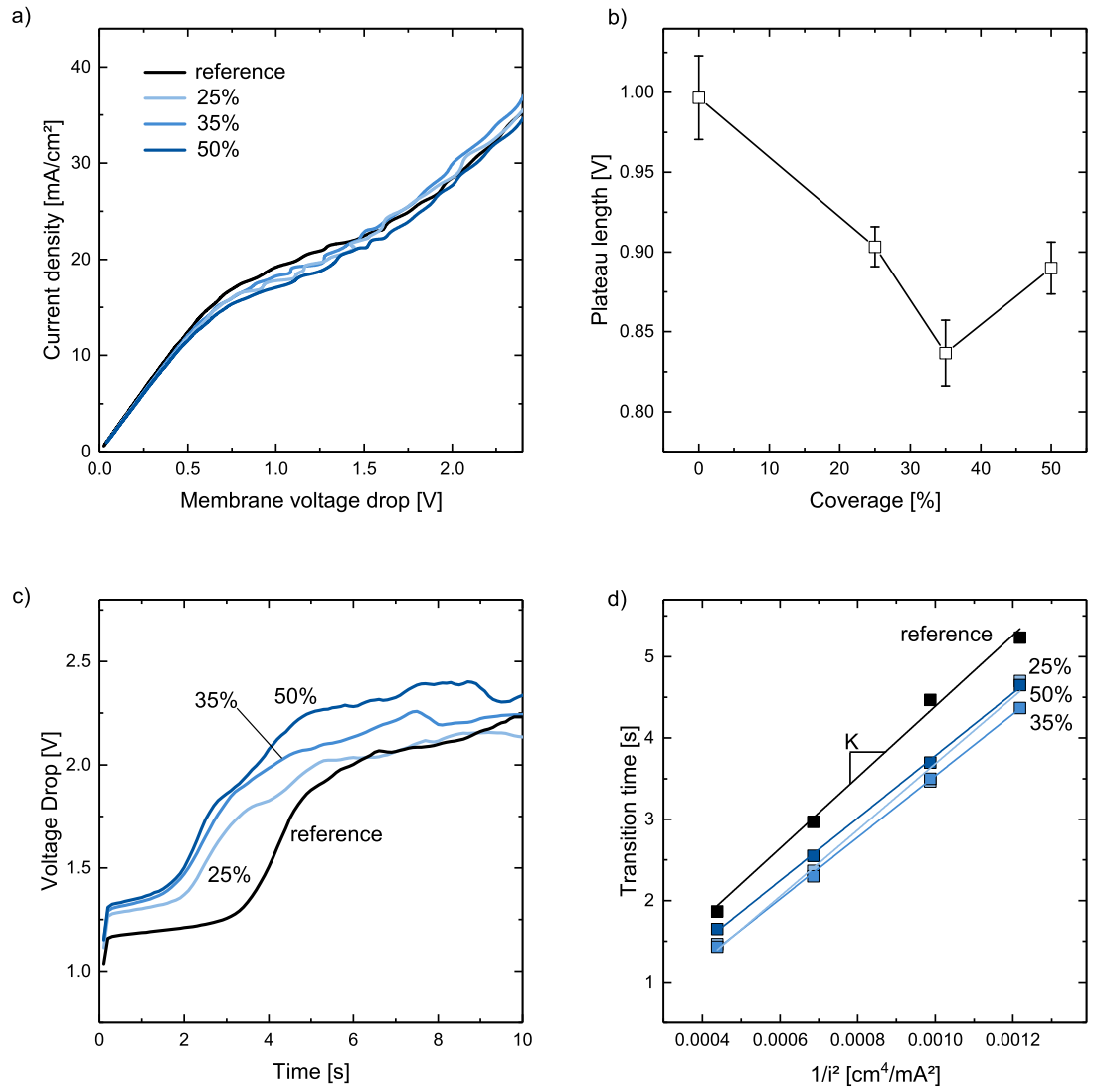

Figure 3: (a) Selected i-V curves of uncoated (reference) and of the polystyrene coated membranes with varying coverage and (b) mean values of the plateau length of all membranes investigated with the same coverage.(c)Chronopotentiometry measurements of selected membranes ink-jet printed with PS at 31$\frac{mA}{cm^2}$ and (d) representation of the mean values of the transition times of all investigated membranes over the reciprocal square of the current density $\frac{1}{i^2}$.

Table 1: Average values of characteristic parameters of the measured current-voltage curves of all investigated polystyrene patterned membranes.

	Ohmic resistance ($\Omega \cdot cm^2$)	Limiting current density ($\frac{mA}{cm^2}$)	Plateau length (V)	Mass transfer constant ($\frac{s \cdot mA^2}{cm^4}$)
Reference	39.4	8.3	1.00	4405
25%	40.5	8.3	0.88	4077
35%	40.5	8.6	0.84	3789
50%	40.6	8.5	0.89	3841

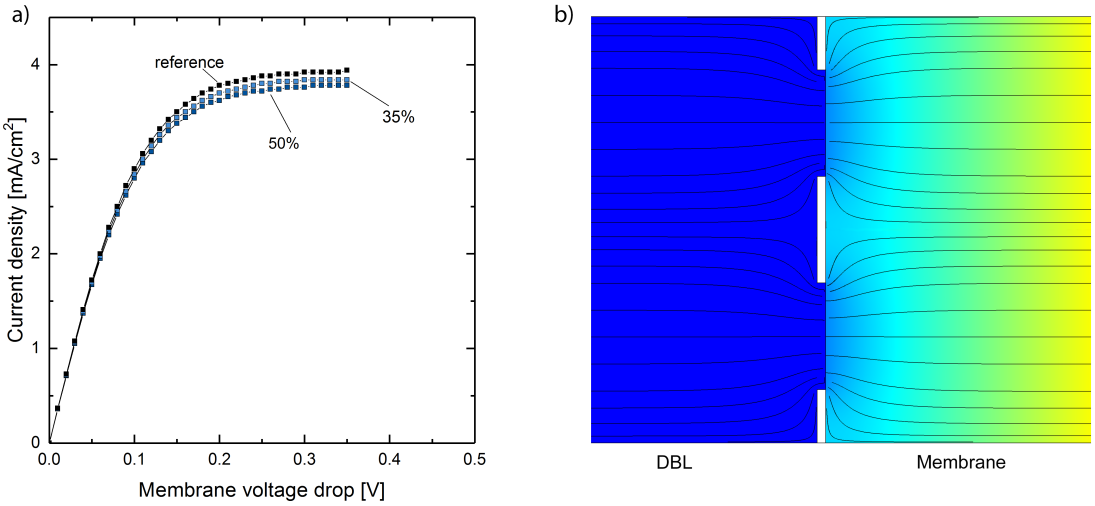

Figure 4: a) i-V curves of membranes with different coverages of impermeable patterns simulated with COMSOL Multiphysics. b) Zoom into the feed-side diffusion boundary layer and the membrane. The electric field lines are deflected by the impermeable patches (white rectangles) and spread into the regions behind the patch inside the membrane again.

the evolution of vortices in the diffusion boundary layer. Figure 3 c shows the voltage response over time of chronopotentiometric measurements of PS-modified membranes and of a reference membrane at 31 $\frac{mA}{cm^2}$. For increased membrane coverage, the transition time diminishes because of the increased local current density in the permeable areas[33].

The Sand equation (Eqn. 1) shows that the transition time is proportional to the reciprocal square of the current density. Substituting all parameters in Equation 1 by a single proportional constant K (Eqn. 4 and 5), this parameter describes the mass transfer towards the membrane up to the inflection point (transition time) of the chronopotentiometric curve.

In Figure 3 d, the transition times of the investigated membranes are, therefore, plotted against the reciprocal square of applied current density, where the slopes of the curves depict the mass transfer parameter K (Table 1).

A comparison of K of the dot-patterned membranes and the reference membranes

shows that the ratio $P = \frac{K_{spot}}{K_{ref}}$ decreases from 0.92 for membranes coated with 25% PS to 0.85 for membranes with 35% and 50% of coverage. In case of impermeable patterns, this apparent decrease in mass transfer is explained by the enlarged current density in the uncovered membrane areas because of the funneling of electric field lines.

In summary, the PS-modified membranes enhance the onset of electroconvection as indicated by the the plateau length reduction up to 15%. Nevertheless, an operation of electrodialyis in the overlimiting region is not favorable with these membranes, since the overlimiting resistance compared to a reference membrane was only slightly reduced.

3.3 P2VP patterns on Nafion

The i-V curves of the membranes modified with linear P2VP polymers also reveal only small increases in the ohmic resistance like the PS patterned ones. However, the P2VP coated membranes show increased limiting current densities (Figure 5 a and Table 3) and a much stronger reduction of the plateau lengths of up to 40% compared to the reference membranes (Figure 5 b). Mishchuk et al. [5] state that the maximum efficiency in an enhanced onset of electroconvection is achieved for significantly different conductivities of patterns and membrane. Since P2VP is partly permeable for ion and the printed geometries are similar to the PS coatings, other properties of the polymers have to cause these drastic changes. The dynamic COMSOL simulations, also accounting for convective fluxes, reveal that the surface charge affects the rotational direction of vortices (Figure 6 b and d). In case of P2VP, the positive surface charge leads to an electrical double layer (EDL) consisting of anions with a positive zeta potential. Here, the electro-osmotic slip is directed such that

the vortices transport the solution from above the patterns towards the pristine membrane (Figure 6 a and b). This reduces the extent of concentration polarization occurring at the patterns since higher concentrated solution is directly transported to the ion transporting domains of the membrane. In addition to this, the velocity of the vortices and the electrical field are directed in the same direction facilitating the ion transport even further.

On the contrary, PS bears a negative surface charge which results in an EDL consisting of cations with a negative zeta potential. Based on our dynamical simulations (Figure 6), the opposite sign of the zeta potential compared to P2VP microgels leads to opposite rotational directions of vortices. As a consequence, at PS patterned membranes, the vortices transport the solution from the pristine membrane surface back towards the non-transporting patterns (Figure 6 c and d). Another drawback of the PS patterns is that the direction of rotation velocity above the pristine membrane is opposite to the direction of the electrical field.

A detailed analysis of the ion transport at the patterned membranes with different surface charges is beyond the scope of this work. Future work will focus on the refinement of the simulations to provide a basis for such an analysis.

The increased limiting currents for the P2VP coated membranes might be explained by the positive surface charge of that polymer. Since the membrane and P2VP bear differently charged EDLs, the charge distribution next to the patterned membranes is highly inhomogenious. These laterally induced concentration polarisations at the membrane-pattern transition are assumed to generate instabilities in the fluid already when the EDL is still in equilibrium so that electroconvection evolves already at underlimiting currents [37].

Table 2: Average values of characteristic parameters of the current-voltage curves of P2VP patterned membranes.

	Ohmic resistance ($\Omega \cdot cm^2$)	Limiting current density ($\frac{mA}{cm^2}$)	Plateau length (V)	Mass transfer constant ($\frac{s \cdot mA^2}{cm^4}$)
Reference	42.4	8.3	0.94	3356
25%	46.9	11.9	0.58	3210
31%	46.1	11.5	0.6	3351

An earlier onset of electroconvective vortices at P2VP modified membranes are also reflected in the results of the chronopotentiometric measurements (Figure 5 c and d). Even though funneling of electric field lines with its associated increased local current density occurs in the pristine membrane areas, the transition times are almost similar to the ones of the reference membranes. The comparison of the mass transfer constants K (slopes of the curves in Figure 5 d, values in Table 2) by $P = \frac{K_{spot}}{K_{ref}}$ reveals an increase in mass transfer for enlarged coverages. P rises from 0.95 for the membranes covered with 25% to 0.99 for coverages of 31%. The latter value reflects almost a similar mass transfer as the reference. In case of higher coverage, the inequality in the EDL grows and thus a more pronounced onset of electroconvective vortices might be induced.

To conclude, the membranes patterned with the linear P2VP polymer increase the limiting current density and reduce the plateau lengths by up to 40% resulting in an enhanced ion transfer in the overlimiting region.

-

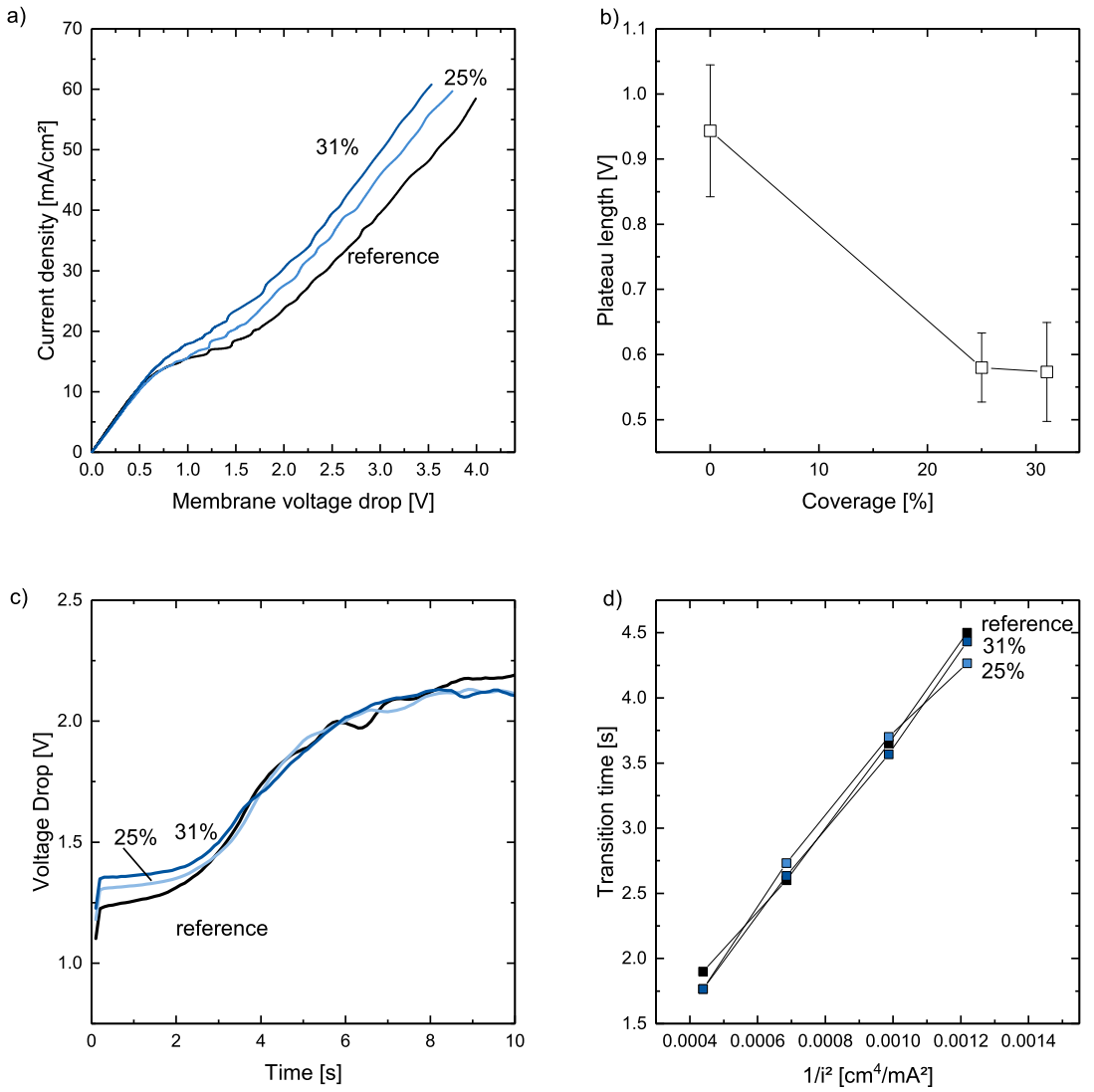

Figure 5: (a) Selected i-V curves of uncoated (reference) and of the P2VP coated membranes with varying coverage and (b) mean values of the plateau length of all membranes investigated with the same coverage.(c)Chronopotentiometry measurements of selected membranes ink-jet printed with P2VP at 31$\frac{mA}{cm^2}$ and (d) representation of the mean values of the transition times of all investigated membranes over the reciprocal square of the current density $\frac{1}{i^2}$.

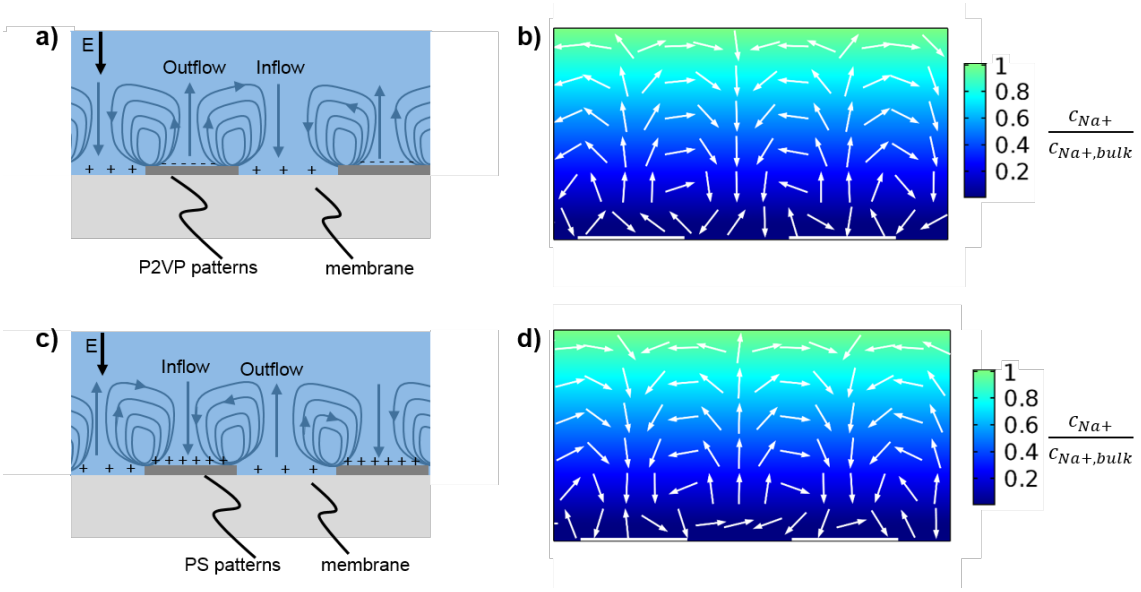

Figure 6: a) Schematic hypothesis of the formation of electroconvective vortices under the influence of an electrical field at P2VP patternend membranes and b) the flow direction of a vortex simulated with COMSOL. c) and d) show the scheme of vortex formation and the simulated results of flow direction of the fluid for membranes coated with PS. In the simulated results, the patches are indicated with the white bars. In the scheme the (+) signs indicate a positive zeta potentials of the surface, the (-) signs a negative zeta potential.

3.4 P2VP microgel patterns on Nafion

As opposed to the surface dots printig from the linear P2VP polymer, the P2VP microgels used in this section consist of crosslinked polymer chains. The P2VP microgels have a spherical shape and are highly water-swollen in free solution. Little is known about the swelling in printed confined layers, certainly not under an electric gradient. In contrast to the linear P2VP polymers forming an homogenous films, the P2VP microgels assemble into monolayer inside a spot with different microgel density distribution shown in (Figure 2 c).

The P2VP microgel coated membranes have ohmic resistances similar to the reference membranes visible by overlapping i-V curves in the underlimiting region in Figure 7 a and in Table 3. The reduction of the plateau length is comparable with

Table 3: Average values of characteristic parameters of the current-voltage curves of P2VP microgel patterned membranes.

	Ohmic resistance ($\Omega \cdot cm^2$)	Limiting current density ($\frac{mA}{cm^2}$)	Plateau length (V)	Mass transfer constant ($\frac{s \cdot mA^2}{cm^4}$)
Reference	39.4	8.3	1.00	4405
25%	39.3	15.7	0.6	4594
31%	39.4	17.7	0.55	6079

that achieved for the spots with the linear P2VP polymers (Figure 7 b).

Also in case of P2VP microgels, such an improvement of ion transport was not predicted since these microgels are neither fully impermeable nor do they completely cover the whole patch.

In the recent past, we have presented confluent monolayers of P2VP microgels coated on Nafion membranes via inclined plane self assembly [29] to investigate the influence of the microgels on the ohmic resistance. In case of these homogeneously covered membranes, the ohmic resistance only increases about 6% compared to a bare membrane. Thus, for the two opposing effects of (a) increasing resistance due to dot coverage and (b) accelarated onset of electroconvection, the latter - induced by different surface charges of PS and P2VP and the inverted rotational direction of vortices for P2VP - dominates the overall mass transport through the concentration polarisation boundary layer and membrane.

The P2VP microgel patterned membranes further reveal even higher limiting current densities than the membranes modified with the linear P2VP, namely of about factor two compared to the reference membranes. In case of the micropatterned areas inside the P2VP microgel spots, the EDL is inhomogeneous on a microscopic level, whereas in case of linear polymers the inhomogeneity is on a macroscopic level only between the 400 μm sized patches and the pristine membrane area. Consequently, the extremely uneven concentration profiles in the micropatterned patches

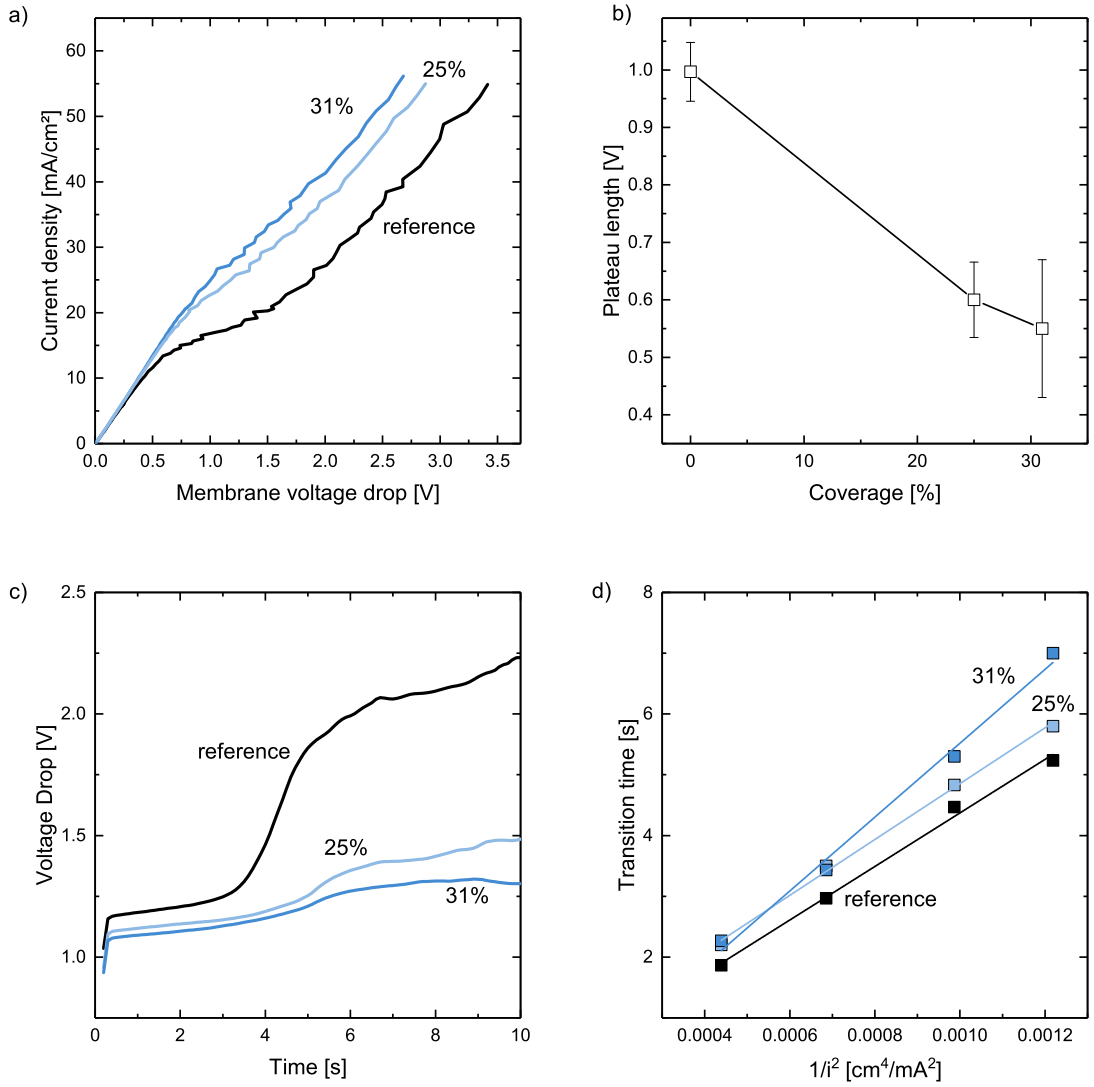

Figure 7: (a)i-V curves of the reference and of the P2VP microgel coated membranes and (b) mean values of the plateau length of all membranes investigated with the same coverage. (c)Chronopotentiometry measurements of selected membranes coated with P2VP microgels at $31\frac{mA}{cm^2}$ and (d) representation of the mean values of the transition times of all investigated membranes over the reciprocal square of the current density $\frac{1}{i^2}$.

might result in an earlier onset of electroconvection even in the underlimiting regime. Such interpretations require extensive experimental and simulative studies beyond the scope of this manuscript.

The associated mass transfer enhancement can also be traced back in the chronopotentiometric measurements (Figure 7 c and d). The transition times are larger compared to the reference indicating that, in this case, electroconvection emerges before the boundary layer is fully depleted and the extended space charge has been fully developed. Analyzing the mass transfer up to the inflection point of the chronopotentiometric curves by P=$\frac{K_{spot}}{K_{ref}}$ (Table 3), we can confirm that the mass transfer in that state of the depletion is enhanced for the membranes coated with P2VP microgels compared to the reference membranes. For the membranes coated with 25% microgels, P has a value of 1.04 and reaches a value of 1.38 for membranes covered with 31% of microgels.

In summary, the P2VP-microgel patterned membranes exhibit an even further enhanced ion transfer in comparison to the linear P2VP dots. Firstly, they show the highest reduction in overall resistance in the overlimiting region of all tested membranes. This renders the suggested method of surface functionalization viable to operate the electrodialysis desalination process in the overlimiting region. Secondly, their limiting current density is twice as high as the one of the reference membranes, so that these microgel-patterned membranes also facilitate an enlarged ion transfer already in the ohmic region. Thus, it is demonstrated that the synergy of the different surface charge of pattern and membrane and the micro structure of the patterns show the biggest mass transfer improvements. Simultaneous pH measurements indicate no water splitting at the membrane surface. Such faradaic side reaction would have reduced current effiency and could have induced scaling

phenomena in real water system. Yet, the absence of pH changes supports technical viability. The results may also encourage the electro-catalysis community to investigate lateral heterogeneity to overcome Nernst polarisation at electrodes.

4 Conclusions

In this paper, the impact of impermeable polystyrene (PS) and poly(2-vinylpyridine) (P2VP) patterns as well as the impact of permeable P2VP microgel patterns on the under- and overlimiting mass transfer was experimentally studied and simulated with COMSOL Multiphysics. Further, the evolution of the electroconvection was investigated. Impermeable PS and P2VP patterns printed on Nafion membranes enlarge the membrane resistance only slightly even though their coverage reached up to 50%. Since the polymer patterns are only coated on top of the membrane, the field lines also spread into the regions behind the patterns once they entered the membrane. Hence almost the whole membrane volume contributes to ion permeation. The PS patterns enhance the mixing of the boundary layer, shown by the up to 15% decreased plateau lengths. Despite this reduction of plateau length, only a slight decrease in overall resistance in the overlimiting regime was achieved.

In contrast to that, P2VP polymer and P2VP microgel patterns of similar dimensions printed on Nafion membranes exhibit enlarged limiting current densities. P2VP microgels patterns doubled the limiting current density because of the formation of lateral microgel density distribution inside of the printed areas. The enhanced mass transfer might be enabled by an evolution of electroconvection already at underliminting currents. Further, a drastic drop in plateau length was achieved. Both types of P2VP patterns reduce the plateau lengths by around 40%. We suggest that these drastic reductions compared to the PS coatings evolve due

to opposite surface charges of the polymers. Time-resolved CFD simulations reveal that the opposite surface charges result in reversed rotational directions of electroconvective vortices contributing to a more efficient mixing of the boundary layer in case of P2VP. We are confident that the first experimental evidence of an improved electroconvection achieved by the synergistic effects of micro patterns and surface charge via microgel coatings will help to (a) further clarify the relevant factors to enhance electroconvection and (b) render electrodialytic desalination processes more efficient.

Supporting Information

Supporting Information is available from the Wiley Online Library or from the author.

Acknowledgements

This work has been supported by the DFG through the project SFB 985 Functional Microgels and Microgel Systems in project C4.This project has also received funding from the European Research Council (ERC) under the European Union's Horizon 2020 research and innovation program (grant agreement no. 694946). The authors acknowledge Elif Karatay, Manuel César Martí Calatayud and Tao Luo for their input and the fruitful discussions.

References

[1] V. V. Nikonenko, A. V. Kovalenko, M. K. Urtenov, N. D. Pismenskaya, J. Han, P. Sistat, G. Pourcelly. *Desalination* **2014**, *342* 85.

[2] J. Balster, M. H. Yildirim, D. F. Stamatialis, R. Ibanez, R. G. H. Lammertink, V. Jordan, M. Wessling. *J. Phys. Chem. B* **2007**, *111* 2152.

[3] I. Rubinstein, B. Zaltzman. *Math. Models Methods Appl. Sci.* **2001**, *11*, 02 263.

[4] I. Rubinstein, F. Maletzki. *J. Chem. Soc., Faraday Trans.* **1991**, *87*, May 2079.

[5] N. A. Mishchuk. *Colloids Surf., A* **1998**, *140*, 1-3 75.

[6] S. Rubinstein, G. Manukyan, A. Staicu, I. Rubinstein, B. Zaltzman, R. Lammertink, F. Mugele, M. Wessling. *Phys. Rev. Lett.* **2008**, *101*, 23.

[7] R. Kwak, G. Guan, W. K. Peng, J. Han. *Desalination* **2013**, *308* 138.

[8] J. C. De Valença, R. M. Wagterveld, R. G. H. Lammertink, P. A. Tsai. *Phys. Rev. E* **2015**, *92*, 3 1.

[9] C. Druzgalski, A. Mani. *Physical Rev. Fluids* **2016**, *1*, 7 073601.

[10] I. Rubinstein, B. Zaltzman. *Phys. Rev. E* **2000**, *62*, 2 2238.

[11] M. Wessling, L. G. Morcillo, S. Abdu. *Sci. Rep.* **2014**, *4* 4294.

[12] N. D. Pismenskaya, N. Melnik, E. Nevakshenova, K. Nebavskaya, V. V. Nikonenko. *Int. J. Chem. Eng.* **2012**, *2012* 528290 .

[13] K. A. Nebavskaya, V. V. Sarapulova, K. G. Sabbatovskiy, V. D. Sobolev, N. D. Pismenskaya, P. Sistat, M. Cretin, V. V. Nikonenko. *J. Membr. Sci.* **2017**, *523* 36.

[14] E. Korzhova, N. D. Pismenskaya, D. Lopatin, O. Baranov, L. Dammak, V. V. Nikonenko. *J. Membr. Sci.* **2016**, *500* 161.

[15] S. M. Davidson, M. Wessling, A. Mani. *Sci. Rep.* **2016**, 1–10.

[16] A. Mikosch, S. Ciftci, A. Kuehne. *ACS Nano* **2016**, *10*, 11 10195.

[17] B.-J. de Gans, P. C. Duineveld, U. S. Schubert. *Adv. Mater. (Weinheim, Ger.)* **2004**, *16*, 3 203.

[18] F. Torrisi, T. Hasan, W. Wu, Z. Sun, A. Lombardo, T. S. Kulmala, G. W. Hsieh, S. Jung, F. Bonaccorso, P. J. Paul, D. Chu, A. C. Ferrari. *ACS Nano* **2012**, *6*, 4 2992.

[19] F. Stumpf, J. Schoendube, A. Gross, C. Rath, S. Niekrawietz, P. Koltay, G. Roth. *Biosens. Bioelectron.* **2015**, *69* 301.

[20] S. Badalov, Y. Oren, C. J. Arnusch. *J. Membr. Sci.* **2015**, *493* 508.

[21] H. Hu, R. G. Larson. *J. Phys. Chem. B* **2006**, *110*, 14 7090.

[22] E. Sowade, T. Blaudeck, R. R. Baumann. *Nanoscale Res. Lett.* **2015**, *10*, 1 362.

[23] M. Orlov, I. Tokarev, A. Scholl, A. Doran, S. Minko. *Macromolecules (Washington, DC, U. S.)* **2007**, *40* 2086.

[24] V. Nerapusri, J. L. Keddie, B. Vincent, I. A. Bushnak. *Langmuir* **2006**, *22*, 11 5036.

[25] B. R. Saunders, N. Laajam, E. Daly, S. Teow, X. Hu, R. Stepto. *Adv. Colloid Interface Sci.* **2009**, *147-148* 251.

[26] R. Tiwari, T. Heuser, E. Weyandt, B. Wang, A. Walther. *Soft Matter* **2015**, *11*, 42 8342.

[27] D. Menne, F. Pitsch, J. E. Wong, A. Pich, M. Wessling. *Angew. Chem., Int. Ed.* **2014**, *53*, 22 5706.

[28] T. Lohaus, P. de Wit, M. Kather, D. Menne, N. E. Benes, A. Pich, M. Wessling. *J. Membr. Sci.* **2017**, *539* 451.

[29] F. Roghmans, M. Martí-Calatayud, S. Abdu, R. Femmer, R. Tiwari, A. Walther, M. Wessling. *Electrochem. Commun.* **2016**, *72* 113.

[30] J. Balster, D. Stamatialis, M. Wessling. *J. Membr. Sci.* **2010**, *360*, 1-2 185.

[31] A. Doyen, C. Roblet, A. L'Archevêque-Gaudet, L. Bazinet. *J. Membr. Sci.* **2014**, *452* 453.

[32] J. J. Krol, M. Wessling, H. Strathmann. *J. Membr. Sci.* **1999**, *162* 155.

[33] N. Pismenskaya, P. Sistat, P. Huguet, V. V. Nikonenko, G. Pourcelly. *J. Membr. Sci.* **2004**, *228* 65.

[34] J.-H. Choi, S.-H. Kim, S.-H. Moon. *J. Colloid Interface Sci.* **2001**, *241*, 1 120.

[35] S. A. Mareev, V. S. Nichka, D. Y. Butylskii, M. K. Urtenov, N. D. Pismenskaya, P. Y. Apel, V. V. Nikonenko. *J. Phys. Chem. C* **2016**, *120*, 24 13113.

[36] V. S. Pham, Z. Li, K. M. Lim, J. K. White, J. Han. *Phys. Rev. E* **2012**, *86*, 4 1.

[37] I. Rubinstein, B. Zaltzman. *Phys. Rev. Lett.* **2015**, *114*, 11 1.

[38] R. Femmer, A. Mani, M. Wessling. *Sci. Rep.* **2015**, *5* 11583.

[39] R. Femmer, M. C. Martí-Calatayud, M. Wessling. *J. Membr. Sci.* **2016**, *520* 29.

[40] E. Karatay, C. L. Druzgalski, A. Mani. *J. Colloid Interface Sci.* **2015**, *446* 67.

[41] C. L. Druzgalski, M. B. Andersen, A. Mani. *Phys. Fluids* **2013**, *25*, 11 110804.